Multidepth, multiparticle tracking for active microrheology using a smart camera

Scott A. Silburn, Christopher D. Saunter, John M. Girkin, and Gordon D. Love
Centre for Advanced Instrumentation and Biophysical Sciences Institute, Department of Physics, Durham University, Durham, DH1 3LE, United Kingdom

(Received 26 January 2011; accepted 23 February 2011; published online 23 March 2011)

The quantitative measurement of particle motion in optical tweezers is an important tool in the study of microrheology and can be used in a variety of scientific and industrial applications. Active microheology, in which the response of optically trapped particles to external driving forces is measured, is particularly useful in probing nonlinear viscoelastic behavior in complex fluids. Currently such experiments typically require independent measurements of the driving force and the trapped particle's response to be carefully synchronized, and therefore the experiments normally require analog equipment. In this paper we describe both a specialized camera and an imaging technique which make high-speed video microscopy a suitable tool for performing such measurements, without the need for separate measurement systems and synchronization. The use of a high-speed tracking camera based on a field programmable gate array to simultaneously track multiple particles is reported. By using this camera to simultaneously track one microsphere fixed to the wall of a driven sample chamber and another held in an optical trap, we demonstrate simultaneous optical measurement of the driving motion and the trapped probe particle response using a single instrument. Our technique is verified experimentally by active viscosity measurements on water–ethylene glycol mixtures using a phase-shift technique. © *2011 American Institute of Physics*. [doi:10.1063/1.3567801]

I. INTRODUCTION

Optical tweezers experiments in microrheology can be classified as using either passive or active measurement techniques to investigate the mechanical properties of viscoelastic fluids.[1] While the former uses the natural Brownian motion of optically trapped probe particles to determine the viscoelastic properties of a medium, the latter uses the response of trapped particles to external driving forces. These active methods are particularly suited to measuring materials' responses to large applied deformations (of the order of microns rather than nanometers for passive methods), as significantly larger probe particle displacements can be achieved. This allows the probing of material properties only exhibited at these larger deformations such as nonlinear behavior in micellar or polymer systems.[2] The control over probe particle velocity offered by active methods also allows the study of further nonlinear effects such as velocity thinning in colloidal suspensions.[3] Active methods are also important in instrument calibration: when working with viscoelastic media of unknown properties, such as the cytoplasm of a living cell, only by a combination of active and passive measurements can *in situ* force calibration of optical tweezers be performed.[4,5] Active calibration and viscosity measurements can also be used for purely viscous media, and optical trap calibration to a precision of 3% has been reported using an active phase-shift-based method.[6]

To use active microrheology it is typically necessary to perform synchronized measurements of an external driving motion and the response of an optically trapped probe particle, in order to compare the two. This is usually achieved by separately measuring the external driving motion and trapped bead position, before comparing or recording the two on a synchronized timebase. Position detection of the trapped particle is typically achieved using a quadrant photodetector (QPD) resulting in an analog voltage, which is then calibrated against the physical displacement of the bead. We shall use the acronym QPD in the remainder of this paper for simplicity but note that other position sensitive detectors exist which are not based on photodiodes. The most common methods of providing the external driving are the use of scanning mirrors to steer the trapping laser beam or the use of a piezoelectric stage to move the sample relative to a fixed trapping point. In the former case, experiments have been demonstrated where the driving motion measurement is derived from the input signal to a beam steering mirror,[7] or from a second QPD configured to detect the position of the trapping laser.[1,2] In the case where a piezoelectric stage is used, the driving motion measurement is derived from feedback signals of the sample stage.[5] The separate driving and bead position measurements are then captured for computer processing via a data acquisition card, or compared in realtime using a lock-in amplifier.[6,7]

These techniques to measure the driving motion present a number of challenges. In order to ensure that the driving and response measurements are properly synchronized, it is necessary to carefully calibrate the latencies involved in the measurements, signal acquisition, and processing. It is also often assumed that the driving or feedback signal accurately represents the physical position of the mirror or sample chamber being driven, which does not take into account mechanical responses of the apparatus. More critically, the techniques only work well with QPDs, but not with imaging detectors as it is very difficult to precisely synchronize data from different detectors. Using cameras to measure particle motion has a number of advantages: they are easier to align, one can simultaneously view the sample and, most importantly, it is

possible to image many particles simultaneously. The combination of bright-field video imaging of trapped beads and single particle tracking has been shown to be capable of temporal sampling of several kilohertz[8] and of reaching nanometer accuracy.[9] Combined with multiparticle optical traps video imaging enables the simultaneous characterization of many locations in a sample.[10] This previous work has involved passive techniques, i.e., no simultaneous monitoring of the stage was necessary. Here we present a video-based detection technique which allows simultaneous optical measurement of the motion of a driven sample stage and the response of an optically trapped particle. This allows us to measure the phase delay between an oscillatory drive and the probe particle response using a single position detection system, with no concern over synchronizing the measurement timebases and providing a direct measurement of the sample chamber position. Furthermore the video imaging system is capable of tracking multiple particles over a wide field of view and does not require the careful alignment of a QPD. First we describe the necessary tracking out-of-focus beads, then present the implementation of a high-speed particle tracking video camera based on field programmable gate arrays (FPGAs). This new method is then applied to multidepth, multiparticle tracking in the context of phase-delay viscosity measurements of water–ethylene glycol mixtures.

II. TRACKING OUT-OF-FOCUS BEADS

Our setup is a conventional optical tweezer system based on an inverted microscope as shown in Fig. 1. The sample chamber is formed using a 175 micron thick glass coverslip, and a CoverWell™ imaging chamber gasket as a protective top cover. For active experiments we require the ability to simultaneously track the trapped particle and the motion of the sample chamber, which is driven by a transducer (not shown in the figure). One could use marks etched onto the sample chamber for tracking; however, we found a better method was to use beads which happen to settle from the sample and stick to the glass coverslip. This avoids the need for nonstandard coverslips, and the fact that the etched marks need to be in the field of view (we did not find it problematic to find beads stuck to the coverslip).

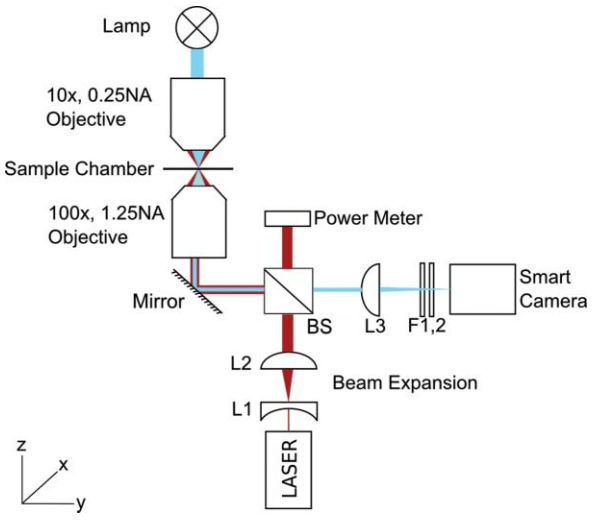

FIG. 1. (Color Online) Schematic diagram of the optical tweezer configuration. The laser beam was expanded by a Galelian telescope, lenses L1 and L2. L3 focused the image of the trapping plane crated by the infinity corrected objective on to the camera. BS: nonpolarizing 50:50 beam splitter, F1,2: 650 nm short-pass filters to protect the camera from backscattered IR laser light. The sample stage was mounted on a piezoelectric translation stage whose axis of motion was aligned in the *y* direction.

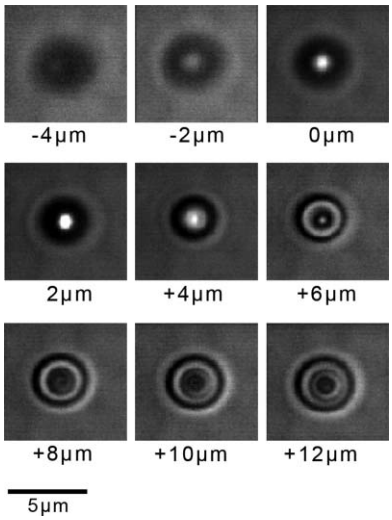

FIG. 2. Images of a 2.85 μm bead taken as the microscope (NA = 1.25) was defocused, in order to simulate the effect of looking at particles at varying depths in the sample for a fixed focus. The numbers refer to the variation in depth (where 0 indicates the in-focus position).

The problem (for either method) is that the trapped particle and the bead stuck to the sample chamber are at different focal depths, and given the small depth-of-field of our system one of them will be severely out of focus. We therefore need a method of tracking both in- and out-of-focus beads. Consider the series of images shown in Fig. 2 which shows the image of a single bead as a microscope is focused in order to simulate the effect of looking at particles at varying depths. Zero depth is defined when the bead is in focus. However, we note that here we see a bright spot surrounded by a dark ring: what we are actually seeing is a focus produced by the bead. More importantly for our purpose here, we note that the out-of-focus images all consist of a dark spot surrounded by brighter rings. The appearance and tracking of out-of-focus beads in microscopes has been considered by a number of authors,[11,12] and the tracking of out-of-focus beads was considered in Ref. 13. Here we use their proposed method of simply inverting the image intensity of an out-of-focus bead before centroiding to find the position.

Figure 3 shows screenshots from our smart camera showing typical images of in- and out-of-focus beads, and the corresponding required image inversion. All images also have a user-defined threshold, which is set in order to remove the effects of background. The use of this software is described more in Sec. IV.

III. SMART CAMERA

We now describe our FPGA-based smart camera used to track beads. FPGAs have previously been used in optical

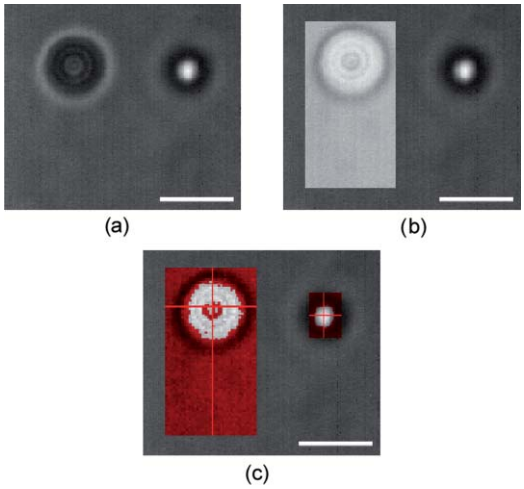

FIG. 3. (Color Online) Particles as imaged by the tracking camera and software. The bead on the right is held by the optical tweezers, while the bead on the left is stuck to the cover glass and appears out of focus. (a) Configuration as seen by the camera. (b) The same image after applying local inversion around the out-of-focus bead. (c) The same image overlayed with the tracking region masking. Red areas are excluded from the centroid calculation, inner unshaded areas contribute to the calculation. White scale bars in all images are 5 μm.

tweezer systems with QPDs (Ref. 14) but here we describe their use in an imaging camera. An FPGA is an integrated circuit containing a number of logic elements which can be reprogramed to implement a specific function. They are programed using a so-called hardware descriptor language. Using a video camera to measure a particle's position generates a significantly larger quantity of data than a QPD. This poses several problems at higher frame rates with the acquisition, movement, and processing of pixel data becoming a problem. A QPD produces two analog signals measuring the x- and y-positions, which can be digitized into two 32-bit floating point values requiring a total of 8 bytes of data per frame. A video-based method using bright-field illumination requires many pixels to image one bead, with typically at least 64 pixels (8×8) being required, producing 128 bytes of data given conventional byte-packing for a typical 10- or 12-bit sensor. Further problems occur when scaling a video-based system to multiple particles, as typically a single rectangular region of the sensor must be read out that encompasses all of the particles, with pixel counts of 10 000s. When reading out at 2 kHz this becomes a significant quantity of data, exceeding the ability of standard computers to acquire, transport, process and store the data.

While most image sensors can only read out the image as a single rectangular array, devices do exist which can read out multiple independent regions. For example the 512×512 CMOS image sensor—"Vanilla" (Ref. 15)—allows access to multiple independent groups of pixels, and has been integrated into a proto-type tweezing system,[16] where six independent regions of 6×6 pixels may be read out for each frame, removing the overabundance of data by leaving just the pixels actually imaging particles. While circumventing the data problem such a system has drawbacks, for example, the loss of wide field video imaging during measurements and a lack of configurability. We have explored a different approach for mitigating the data-rate problems. The speed and frame rate with which a CMOS sensor may be read out is not the primary bottleneck. A typical CMOS sensor can read pixels out at 10–20 Mpixels/s per readout channel, and many readout channels can be combined for parallel readout to produce a multiported chip with very high framing rates. Examples include the Sony IMX017CQE sensor which achieves 632 Mpixels/s and the Cypress LUPA-300 device which achieves 80 Mpixels/s.

We have identified that while there is a great benefit in receiving images from a camera for multiparticle tracking, this is primarily for human use in visual alignment and setup and to provide experimental context, such as ensuring that adjacent particles are not drawn into an active trap during a measurement. Thus there is no need for the images themselves to be transmitted to a computer and displayed faster than around 10 Hz. At the higher sampling speeds it is only the positions of particles within the video image that are important. With this in mind we have created a *smart camera* that uses onboard processing to measure the centroid positions of particles within the camera at high frame-rates. These high-speed centroids are then returned to the computer in parallel with a sub-set of the images from which they were measured, providing a 10 Hz display of the video feed.

Figure 4 provides an overview of dataflow through our camera. The entire system operates on live streaming pixel data rather than images stored in memory. Pixels stream from the CMOS sensor into a Virtex-4 LX40 FPGA. We subtract the fixed pattern noise from the image using a look-up table of per-pixel offsets stored in an external static random access memory (SRAM) memory. This is necessary as the LUPA-300 image sensor suffers from significant fixed pattern noise which on average consumes 15% of the dynamic range of the sensor. The pixel data are then split into two identical streams. One of these undergoes a down-selection process that only allows around 10 frames/s through. The second pixel stream is processed by a centroider which measures the cenetr-of-mass of a series of programmable regions and outputs only the measured centroids. Both the down-selected images and the centroids are then gathered and buffered into the external SRAM which is continuously readout over a USB2 interface by a host computer where they are displayed on a graphical user interface (GUI) and may be recorded to disk. The GUI is also used to configure the camera, including the position and speed of the readout window and the areas processed by the centroider. The GUI was produced with the PYTHON language and the wxPython interface library. Centroids are recorded to disk in a text format along with frame counts and timestamps. Further data processing and analysis was performed in MATLAB. Custom printed circuit boards including the FPGA, SRAM, USB2 interface device, and auxiliary chips were created for the camera by Enterpoint Ltd., derived from their Broaddown4 Virtex-4 device. These were packaged inside an aluminum enclosure of dimensions 140 mm $\times$ 110 mm $\times$ 45 mm with a standard C mount to form a compact smart camera.

The centroider module is derived from an earlier system for measuring the position of bright spots in a Shack–Hartmann wavefront sensor[17] for adaptive optics. [18] The centroider measures the optical center of mass of up to 16

TABLE I. Achievable frame rates for tracking with our smart camera.

Width (pixels)	Height (pixels)	Frame rate (Hz)
16	16	50 000
32	32	25 000
64	64	10 000
128	128	3 300
32	8	60 000

user-programmable regions of arbitrary size from 2×2 to 256×256 pixels and the regions may be overlapping or separate. The regions are grouped into four groups of four and each grouping has a user-programmable background subtraction threshold to isolate the images of beads from the background bright-field illumination. The centroider module can also invert user-selected rectangular regions in order to track out-of-focus images, as described in Sec. II.

Given sufficient illumination, the maximum speed at which one or more particles can be tracked is decided by size of the rectangular area of pixels bounding all particles—see Table I for some examples. As an illustration a single particle confined within a 16×16 pixel block could be tracked at 50 kHz and 16 particles could be tracked at 10 kHz within an area of 64×64 pixels.

IV. EXPERIMENTAL DEMONSTRATION

We now describe the use of our camera to simultaneously image two beads at different depths in order to perform active viscosity measurements on a water–ethylene glycol mixture. For sinusoidal external driving of the sample with amplitude A_0 and frequency f, the equation of motion of an optically trapped bead of mass m in a purely viscous material is given by,[7]

$$m\frac{d^2x}{dt^2} + \gamma\frac{dx}{dt} + \kappa x = \kappa A_0 \sin(2\pi f t), \tag{1}$$

where x is the position of the bead along the driving axis, t is time, γ is the drag coefficient of the bead given by Stokes' law, and κ is the force constant of the optical trap. This gives the response of the bead to be,

$$x(t) = \frac{A_0 f}{\sqrt{f_c^2 + f^2}} \sin(2\pi f t - \delta), \tag{2}$$

where f_c is the characteristic corner frequency of the system. For the case of overdamped motion the phase shift δ is given by

$$\delta \approx \arctan\left(\frac{f_c}{f}\right). \tag{3}$$

The phase shift can therefore be used to obtain the corner frequency f_c, which contains information about the viscosity of the fluid and stiffness of the optical trap. For an optical trap of known stiffness, the corner frequency can be used to calculate the viscosity, η, of the fluid via,

$$\eta = \frac{\kappa}{12\pi^2 f_c r}, \tag{4}$$

where r is the radius of the trapped particle (this expression is only applicable for spherical particles).

Mixtures of de-ionized water and 1,2-Ethanediol [Sigma 293237] were prepared containing mole fractions of ethanediol equal to 0.2 , 0.4 , 0.6, and 0.8. Melamine Formaldehyde microspheres of diameter 2.85 μm $\pm$1% [Corpuscular C-MF-3.00] were diluted in these mixtures to be used as the probe particles.

Measurements were performed using the optical tweezers configuration shown schematically in Fig. 1. The trapping

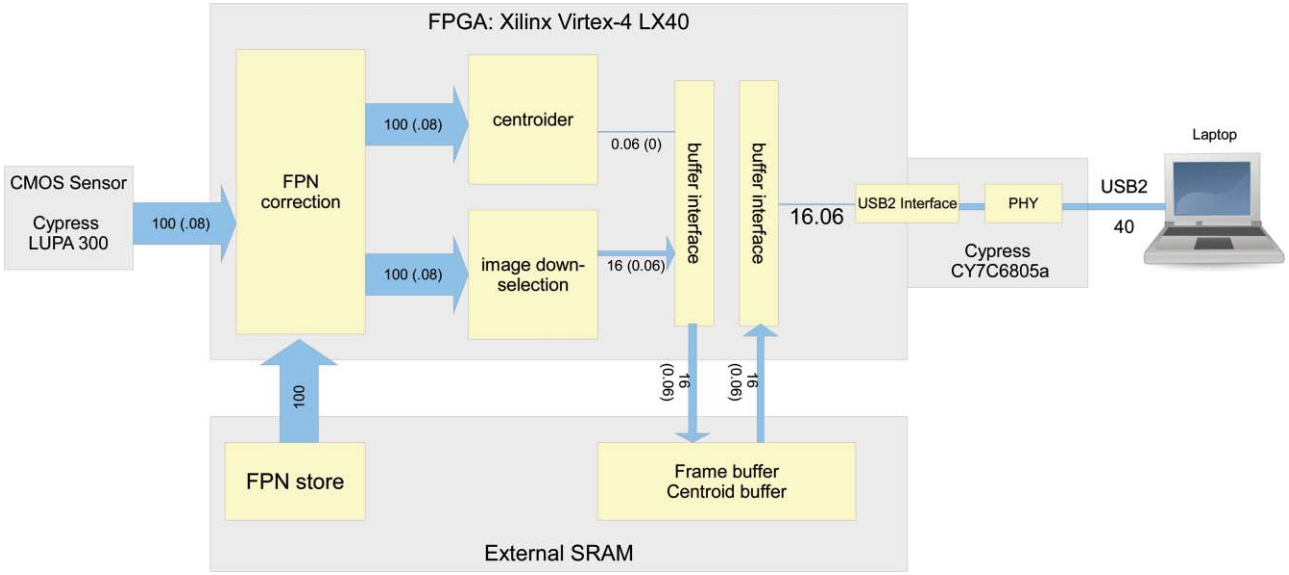

FIG. 4. (Color Online) Dataflow through the various microchip devices forming our smart camera. The thickness of the arrows relates to the quantity of data, with the data rate being shown in MB/s (KB/frame inside the brackets). Images travel from the CMOS sensor to the FPGA where fixed pattern noise is removed. The datastream is then split with a "centroider" module measuring the positions of objects within all the images. These centroids are buffered in an external SRAM memory along with a down-selected subset of images, both of which are then transmitted to a PC over USB2.

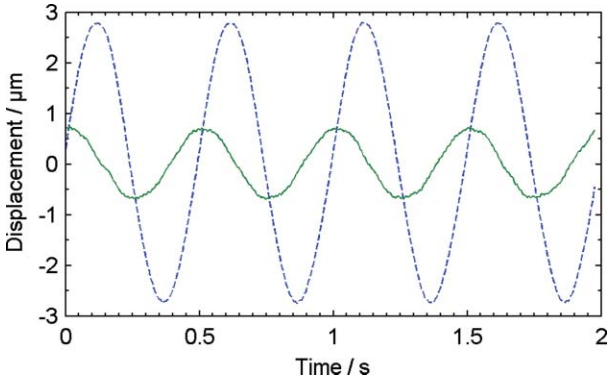

FIG. 5. (Color Online) Simultaneously recorded displacements of a settled reference bead (dashed line) and of an optically trapped probe bead (solid line) in the 0.8 mole fraction water–glycol mixture. The sample stage was driven sinusoidally at 2 Hz and the motion recorded at 250 Hz.

force was provided by a 1W Nd:YAG laser [LCS-DTL-322, Laser 2000 UK Ltd.] which, after beam expansion, was focused using a 100 × 1.25 NA oil immersion microscope objective in an inverted configuration. The objective was used both to create the optical trap and image the trapping plane on to the camera, with sample illumination provided by a tungsten-halogen lamp focused on the sample using a 10 × 0.25 NA objective. The sample chamber consisted of a glass microscope coverslip and CoverWell™imaging chamber gasket, between which the sample was placed. This was mounted on a single-axis piezoelectric translation stage [Physik Instrumente P-625.1CD] controlled by computer via a RS232 to achieve active driving. The force constant κ of the optical trap was calibrated individually for each measurement using the equipartition method.[19] Values of κ used in the measurements were typically around 16 pN/μm. The sample temperature was measured using a K-type thermocouple in direct contact with the liquid sample.

We used our method of simultaneously imaging both a trapped particle and a particle stuck to the sample chamber coverslip. In order to avoid the proximity of the trapped probe bead to the sample chamber wall affecting the viscosity measurements, the probe particle was held approximately 15 μm above the glass coverslip. The appearance of the trapped and stuck beads is shown in Fig. 3. The piezoelectric stage was driven sinusoidally with a peak-to-peak amplitude of approximately 5 μm at a frequency of 2 Hz. The positions of the trapped and reference beads were simultaneously recorded over 20 cycles of the motion at a frame rate of 250 Hz. The phase shift between the reference and trapped bead motions was then found by fitting each bead's recorded position with a wave of the form $A\sin(2\pi f t + \phi)$ and subtracting the two resulting values of ϕ. This was then used to calculate the corner frequency f_c and viscosity η of the mixture using Eqs. (3) and (4), respectively.

TABLE II. Results of active phase-shift viscosity measurements of water–ethanediol mixtures using our techniques compared with bulk values measured using a falling-cylinder viscometer (Ref. 20).

Mole fraction Ethanediol	Bulk viscosity (mPa s)	Active result (mPa s)
0.2	2.925	3.1 ± 0.5
0.4	5.764	4.7 ± 0.5
0.6	9.207	10.0 ± 1.0
0.8	13.10	13.4 ± 1.1

Using measurements on dry beads fixed to the sample chamber coverglass, the root-mean-square (rms) noise on tracking in-focus beads was compared to that when using the inverted tracking on beads 5–10 μm in front of the focal plane. The inverted tracking was found to have rms noise of 10.1 nm averaged over all of the beads recorded, while the noise on in-focus beads was on average 1.8 nm. This difference, of approximately a factor of five, is attributed to the lower contrast of the out-of-focus bead images compared with the in-focus case. In both cases the noise was much smaller than the displacements measured in the viscosity measurements, which was of the order of microns.

In order to confirm that the reference beads were moving in-phase with the sample chamber coverglass, a specially patterned coverslip, with lithographically deposited silver marks which could be tracked by the camera, was incorporated into the sample chamber, and the positions of settled beads and the coverglass were tracked simultaneously under the same driving as used in the viscosity measurements. The settled beads were found to oscillate in-phase with the patterned sample chamber to within the fitting errors, confirming that they provided a valid reference for sample chamber motion.

Figure 5 shows an example of simultaneously recorded trapped and reference bead displacements, measured in the 0.8 mole fraction solution. A well-defined phase shift is seen between the two, and from the sinusoidal fitting the phase difference δ was determined in all the mixtures with relative errors between 0.5–1.5%.

The resulting calculated viscosities for the mixtures are shown in Table II, alongside bulk values from the literature measured using a falling cylinder viscometer.[20] The values obtained with our method are in agreement within their experimental errors with the bulk values, with the exception of the 0.4 mole fraction mixture.

The errors of approximately 10% on the final viscosity values arise mainly from the equipartition calibration of the optical trap stiffness, which itself had a relative error of approximately 8%.

V. CONCLUSIONS

We have presented the implementation of a high-speed, multiparticle tracking camera suitable for microrheological measurements in optical tweezers. By applying a simple image inversion technique, we have demonstrated simultaneous tracking of microspheres at physical depths separated by up to 15 μm using this camera, with rms noise of the order of 10 nm. By using this technique to simultaneously track one microsphere held in optical tweezers and another stuck to the coverglass of a driven sample stage, we have demonstrated phase-delay-based active viscosity measurements without the need for separate measurement systems and synchronization. This is experimentally simpler than traditional active

microrheology techniques and provides a direct measurement of the sample stage motion; this could allow these experiments to be performed with an uncalibrated sample stage. The technique is limited to the regime whereby the stage can be driven at a sufficiently high frequency. The technique could also be easily generalized to perform multipoint measurements, using the camera's multiparticle tracking ability. Apart from the tracking camera itself our technique requires no specialized optics or hardware.

ACKNOWLEDGMENTS

We thank Martin Booth and Tony Wilson (Oxford) and Richard Bowman and Miles Padgett (Glasgow) for pointing out some useful references. We also thank Jonathan Taylor for experimental help with the optical tweezers and Andrew Gallant who fabricated the patterned microscope coverslips. C.D.S acknowledges support from a British Heart Foundation Excellence Award.

[1]R. R. Brau, J. M. Ferrer, H. Lee, C. E. Castro, B. K. Tam, P. B. Tarsa, P. Matsudaira, M. C. Boyce, R. D. Kamm, and M. J. Lang, J. Opt. A, Pure Appl. Opt. **9**, 103 (2007).
[2]H. Lee, J. M. Ferrer, F. Nakamura, M. J. Lang, and R. D. Kamm, Acta Biomater. **6**, 1207 (2010).
[3]I. Sriram, A. Meyer, and E. M. Furst, Phys. Fluids **22**, 062003 (2010).
[4]M. Fischer and K. Berg-Sørensen, J. Opt. A, Pure Appl. Opt. **9**, 239 (2007).
[5]M. Fischer, A. C. Richardson, S. N.S. Reihani, L. B. Oddershede, and K. Berg-Sørensen, Rev. Sci. Instrum. **81**, 015103 (2010).
[6]Z. Ding, G. Lai, T. Sakakibara, and S. Shinohara, J. Appl. Phys. **88**, 737 (2000).
[7]M. Valentine, L. Dewalt, and H. Ou-Yang, J. Phys. Condens. Matter **8**, 9477 (1996).
[8]S. Keen, J. Leach, G. Gibson, and M. J. Padgett, J. Opt. A, Pure Appl. Opt. **9**, S264 (2007).
[9]G. Gibson, J. Leach, S. Keen, A. Wright, and M. J. Padgett, Opt. Express **16**, 405 (2008).
[10]R. Di Leonardo, S. Keen, J. Leach, C. D. Saunter, G. D. Love, G. Ruocco, and M. J. Padgett, Phys. Rev. E **76**, 61402 (2007).
[11]W. Weise, P. Zinin, T. Wilson, A. Briggs, and S. Boseck, Opt. Lett. **21**, 1800 (1996).
[12]S. Lee and D. Grier, Opt. Express **15**, 1505 (2007).
[13]Z. Zhang and C. Menq, Appl. Opt. **47**, 2361 (2008).
[14]T. Aggarwal and M. Salapaka, Rev. Sci. Instrum. **81** (2010).
[15]A. Blue, R. Bates, S. Bohndiek, A. Clark, C. Arvanitis, T. Greenshaw, A. Laing, D. Maneuski, R. Turchetta, and V. Oshea, Nucl. Instrum. Methods Phys. Res. A **591**, 237 (2008).
[16]M. Towrie, S. W. Botchway, A. Clark, E. Freeman, R. Halsall, A. W. Parker, M. Prydderch, R. Turchetta, A. D. Ward, and M. R. Pollard, Rev. Sci. Instrum. **80**, 103704 (2009).
[17]C. D. Saunter, G. D. Love, M. Johns, and J. Holmes, Proc. SPIE **6018** (2005).
[18]M. Langlois, C. D. Saunter, C. N. Dunlop, R. M. Myers, and G. D. Love, Opt. Express **12**, 1689 (2004).
[19]K. C. Neuman and S. M. Block, Rev. Sci. Instrum. **75**, 2787 (2004).
[20]Y. Tanaka, K. Ohta, H. Kubota, and T. Makita, Int. J. Thermophys. **9**, 511 (1988).